



Multi-wavelength analytical ultracentrifugation as a tool to characterise protein–DNA interactions in solution

Christopher R. Horne¹  · Amy Henrickson²  · Borries Demeler²  · Renwick C. J. Dobson^{1,3} 

Received: 30 September 2020 / Accepted: 9 November 2020 / Published online: 21 November 2020
© European Biophysical Societies' Association 2020

Abstract

Understanding how proteins interact with DNA, and particularly the stoichiometry of a protein–DNA complex, is key information needed to elucidate the biological role of the interaction, e.g. transcriptional regulation. Here, we present an emerging analytical ultracentrifugation method that features multi-wavelength detection to characterise complex mixtures by deconvoluting the spectral signals of the interaction partners into separate sedimentation profiles. The spectral information obtained in this experiment provides direct access to the molar stoichiometry of the interacting system to complement traditional hydrodynamic information. We demonstrate this approach by characterising a multimeric assembly process between the transcriptional repressor of bacterial sialic acid metabolism, NanR and its DNA-binding sequence. The method introduced in this study can be extended to quantitatively analyse any complex interaction in solution, providing the interaction partners have different optical properties.

Keywords Multi-wavelength analytical ultracentrifugation · Protein–DNA interaction · Sedimentation velocity · NanR · Sialic acid

Introduction

Regulating gene expression is a fundamental process that enables bacteria to adapt to environmental stresses, such as changes in nutrient availability (de Lorenzo and Cases 2005; Deutscher 2008; Gorke and Stulke 2008). On a molecular level, this process is orchestrated by transcriptional regulators, which induce expression of the appropriate metabolic

machinery in response to environmental cues, for example, the presence or absence in the environment of particular sugars (Bervoets and Charlier 2019; Gerosa et al. 2013). To aid a functional understanding of how transcriptional regulators mediate this biological process, validation of the stoichiometry involved in protein–DNA binding and insight towards the thermodynamics of the respective interaction is essential.

Analytical ultracentrifugation (AUC) is the gold-standard technique to quantitatively characterise molecules or molecular interactions in the solution environment. Notably, AUC combines the power of a centrifuge and an optical system to analyse the sedimentation and diffusion behaviour of molecules under biologically-relevant buffer conditions (e.g. pH, reducing potential and ionic strength) (Cole et al. 2008) and recent work has begun to address hydrodynamic properties in complex solutions, such as cell lysates (Kroe and Laue 2009). Based on first principles, the experiment provides access to the size distribution, shape and molecular weight of the molecules in solution, along with the dynamics of the system, such as a good estimation of binding constants within a self-associating system or ligand binding (Demeler 2010).

AUC data can be collected in real time using the UV/Vis absorbance, Rayleigh interference, or fluorescence emission

Special Issue: Analytical Ultracentrifugation 2019.

Electronic supplementary material The online version of this article (<https://doi.org/10.1007/s00249-020-01481-6>) contains supplementary material, which is available to authorized users.

✉ Renwick C. J. Dobson
renwick.dobson@canterbury.ac.nz

¹ Biomolecular Interaction Centre and School of Biological Sciences, University of Canterbury, PO Box 4800, Christchurch 8140, New Zealand

² Department of Chemistry and Biochemistry, University of Lethbridge, Lethbridge, AB T1K 3M4, Canada

³ Department of Biochemistry and Molecular Biology, Bio21 Molecular Science and Biotechnology Institute, University of Melbourne, Parkville, VIC 3010, Australia

optical systems (Cole et al. 2008; Demeler 2010). Each method has been successfully employed to characterise protein–DNA interactions in solution [for representative studies, we refer the reader to Laue et al. (1993), Lee et al. (2001), Witte et al. (2005) and Yang et al. (2015)], although there are some shortcomings/limitations. For example, because single-wavelength studies (e.g. measuring at 280 nm) cannot separate the signals from protein and DNA, up to three different wavelengths can be selected using the Beckman-Coulter XL-A/I absorbance system, and the XL-I also enables Rayleigh interference data to be collected at the same time (Berke and Modis 2012). However, this multi-signal approach is impractical as the XLA/I instruments do not reproducibly return to the same wavelength after each scan and spectral resolution is poor due to hardware limitations. In contrast, the fluorescence optical system offers superb sensitivity and selectivity, enabling reliable measurements down to picomolar concentrations within complex solutions (MacGregor et al. 2004; Zhao et al. 2014), but one of the interacting partners must be extrinsically labelled with a fluorescent probe that is compatible with the excitation laser (488 nm), which may introduce confounding factors to the experiment. Furthermore, care must be taken when operating at very low concentrations to avoid sample sticking to the surface of the ultracentrifuge cell, and the addition of a non-labelled ‘carrier’ protein (e.g. bovine serum albumin, or kappa casein) to the sample buffer helps prevent this (Demeler 2010). Collectively, these limitations restrict our ability to accurately characterise the interactions between dissimilar molecules within a complex mixture.

The new Beckman-Coulter Optima AUC instrument features multi-wavelength detection (Pearson et al. 2015), which is ideal for studying protein–DNA interactions in solution. The ability to collect data over multiple wavelengths during the same run introduces an additional spectral dimension, which substantially increases the data density and leads to a significant improvement in resolution over single-wavelength methods (Gorbet et al. 2015). While the increased data density presents an additional challenge, data analysis is manageable with the UltraScan software package, which utilises parallel distributed computing to tackle the computational load (Demeler et al. 2009; Demeler and Gorbet 2016). Notably, this analysis allows the overlapping signals of protein and DNA to be deconvoluted into separate profiles, based on their spectral differences, providing direct access to the molar stoichiometry of interacting complexes, along with complementary hydrodynamic information for each component.

To illustrate the potential of this next-generation approach, we investigate the interaction between the transcriptional repressor of bacterial sialic acid metabolism, NanR and its cognate DNA-binding sequence. Sialic acids are a family of negatively-charged, amino sugars that

decorate the surface of mammalian cells, where they mediate a variety of recognition and adhesion processes (Baos et al. 2012; North et al. 2018a; Vimr et al. 2004). Pathogenic and commensal bacteria that colonise sialic acid-rich environments have evolved elaborate mechanisms to utilise host-derived sialic acids as a source of nutrition for a competitive advantage (Almagro-Moreno and Boyd 2009; Vimr 2013). We have been engaged in series of studies that examine how sialic acid is metabolised by bacteria, focusing on the mechanism of sialic acid import (North et al. 2018a, b; Wahlgren et al. 2018) and its subsequent enzymatic degradation (Coombes et al. 2020; Davies et al. 2019; Horne et al. 2019; North et al. 2016). Here, we shift focus to examine the mechanism of pathway regulation. The gene expression of the sialic acid metabolic machinery is regulated by the transcriptional repressor, NanR (Horne et al. 2020; Kalivoda et al. 2003). Our previous work has shown that NanR from *Escherichia coli* achieves gene repression by cooperatively binding a (GGTATA)₃-repeat operator with high affinity. This interaction involves three NanR dimers in an elaborate, multimeric assembly process (Horne et al. 2020). As a case study for multi-wavelength AUC, we characterise the interaction between NanR and an oligonucleotide with two repeats, i.e. (GGTATA)₂-repeat.

Materials and methods

Protein expression and purification

DNA encoding wild-type NanR from *E. coli* (synthesised by GenScript) (UniProt accession-P0A8W0) was cloned into a pET28a expression vector and then transformed into *E. coli* BL21(DE3) cells. Cells were cultured in Luria–Bertani growth medium supplemented with kanamycin (30 µg mL⁻¹) and ZnCl₂ (100 µM) at 37 °C with shaking at 220 rpm to an OD₆₀₀ of ~0.6. Protein expression was induced by the addition of isopropyl β-D-1-thiogalactopyranoside to 1 mM and the temperature was lowered to 26 °C for incubation overnight. Cell pellets were resuspended in lysis buffer (20 mM Tris–HCl (pH 8.0), 150 mM NaCl, 100 µM ZnCl₂), supplemented with Complete protease cocktail inhibitor (Roche), and lysed by sonication. Cell debris was separated from soluble protein by centrifugation at 18,000 rpm. NanR was purified using a four-step procedure: ammonium sulphate precipitation, anion-exchange, heparin-affinity and size-exclusion chromatographies using the ÄKTApure chromatography system (Cytiva), as described previously in Horne et al. (2020). Proteins that eluted from the size-exclusion column were assessed for purity by SDS-PAGE. Protein that was not immediately used in experiments was flash-frozen in liquid nitrogen and stored at –80 °C.

Double-stranded DNA formation

Complementary DNA oligonucleotides (Integrated DNA Technologies) were resuspended in a buffer consisting of 20 mM Tris–HCl (pH 8.0), and 150 mM NaCl, mixed at equimolar concentrations, and then hybridized by heating to 95 °C for 5 min, followed by cooling slowly to room temperature. For electrophoretic mobility shift assays, DNA oligonucleotides were FAM-5′-labelled on both strands to improve sensitivity, while DNA for AUC experiments were unlabelled. Double-stranded DNA oligonucleotides were stored at –20 °C until use.

Electrophoretic mobility shift assays

FAM-5′-labelled (GGTATA)₂-repeat DNAs were diluted to 10 nM in gel shift buffer (10 mM MOPS (pH 7.5), 50 mM KCl, 5 mM MgCl₂, and 10% (v/v) glycerol). Twelve-well Novex 6% Tris–glycine gels (Invitrogen) were pre-run in 0.5 × Tris–Borate–EDTA (TBE) buffer (40 mM Tris–HCl (pH 8.3), 45 mM boric acid, and 1 mM EDTA) at 200 V for 30 min at 4 °C. NanR was titrated against the (GGTATA)₂-repeat DNA and incubated at room temperature for at least 30 min to allow samples to reach equilibrium. Electrophoresis was performed immediately on the pre-run gels in 0.5 × TBE buffer at 200 V for 20 min at 4 °C. Gels were imaged using a Typhoon FLA 9500 Biomolecular Imager (GE Healthcare) with a 473 nm excitation source and a long-pass emission filter.

Multi-wavelength analytical ultracentrifugation: data collection

Multi-wavelength sedimentation velocity experiments were performed in a Beckman Coulter Optima analytical ultracentrifuge using double-sector epon-charcoal centre-pieces fitted with quartz windows in an An-60 Ti four-hole rotor at 20 °C. Initially, purified NanR and double-stranded (GGTATA)₂-repeat DNA were extensively dialyzed against a buffer containing 50 mM sodium phosphate (pH 7.4), and 150 mM NaCl. Phosphate was chosen to minimize background absorbance and, therefore, maximize signal from the protein and DNA. Individual control experiments were performed by measuring separately NanR (12 μM) and (GGTATA)₂-repeat DNA (1.2 μM) at 280 and 260 nm, respectively. Samples were then prepared with increasing loading concentrations of NanR (1.2, 2.4, 4.8, 7.2 and 12 μM) with respect to (GGTATA)₂-repeat DNA (1.2 μM). Data were collected at either 50,000 or 60,000 rpm and sedimentation was monitored using the UV absorption system in intensity mode, scanning only a single double-sector cell with two samples, one in each sector. Sedimentation velocity scans were recorded in the range of 220–300 nm with 2 nm

increments, providing 41 individual datasets for each loading concentration. All data were analysed using UltraScan 4.0 (Demeler and Gorbet 2016).

Multi-wavelength analytical ultracentrifugation: data analysis workflow

The multi-wavelength sedimentation velocity datasets from each wavelength were analysed using 2DSA (Brookes et al. 2010) to remove systematic noise components, and to determine boundary conditions of the sample column as reported above. Iteratively refined 2DSA models from each wavelength were used to generate a sedimentation profile for each wavelength mapped to a common time grid. Spectral deconvolution of the multiwavelength data using the molar extinction coefficient profiles of each spectral contributor generates spectrally separated hydrodynamic results for each contributor. The partial specific volume for NanR was predicted based on the amino acid sequence of NanR using UltraScan, and by assuming a partial specific volume of 0.55 mL g⁻¹ for DNA and using the determined stoichiometry to calculate a weight-average partial specific volume (see below). Buffer density and viscosity were determined based on the buffer composition using UltraScan.

Molar extinction profiles were determined by performing separate dilution series for both NanR and DNA, collecting an absorbance spectrum across the spectral range of interest (220–300 nm) using a Genesys 10 s benchtop spectrophotometer (Thermo Fisher Scientific). The dilution series of each absorbance spectrum was fitted to intrinsic extinction profiles as described previously (Fig. 1) (Gorbet et al. 2015; Zhang et al. 2017). The resulting intrinsic extinction profiles were scaled to molar concentration using an extinction coefficient of 13,980 M⁻¹ cm⁻¹ at 280 nm for wild-type NanR as calculated by ExPASy ProtParam from the amino acid sequence. For the (GGTATA)₂-repeat oligonucleotide, an extinction coefficient of 276,816 M⁻¹ cm⁻¹ at 260 nm was determined by the nearest-neighbour method (Fasman 1975). The vector angle between these spectral profiles was 60.2°, which represents good orthogonality between spectra and therefore ensures separability. An angle of 0° reflects linear dependence or perfect overlap, while an angle of 90° indicates perfect orthogonality—no spectral overlap. Next, the spectral profiles, scaled to molar concentration, were used to deconvolute the noise-corrected multiwavelength data into separate datasets for the NanR and DNA components using the non-negatively constrained least squares algorithm (Lawson and Hanson 1974) as previously described (Gorbet et al. 2015; Zhang et al. 2017). This spectral decomposition is illustrated in Fig. 1. These deconvoluted datasets were individually analysed by the iterative 2DSA method using UltraScan (Brookes et al. 2010). The resulting amplitudes of the deconvoluted species involved in hetero-complex formation were then integrated to

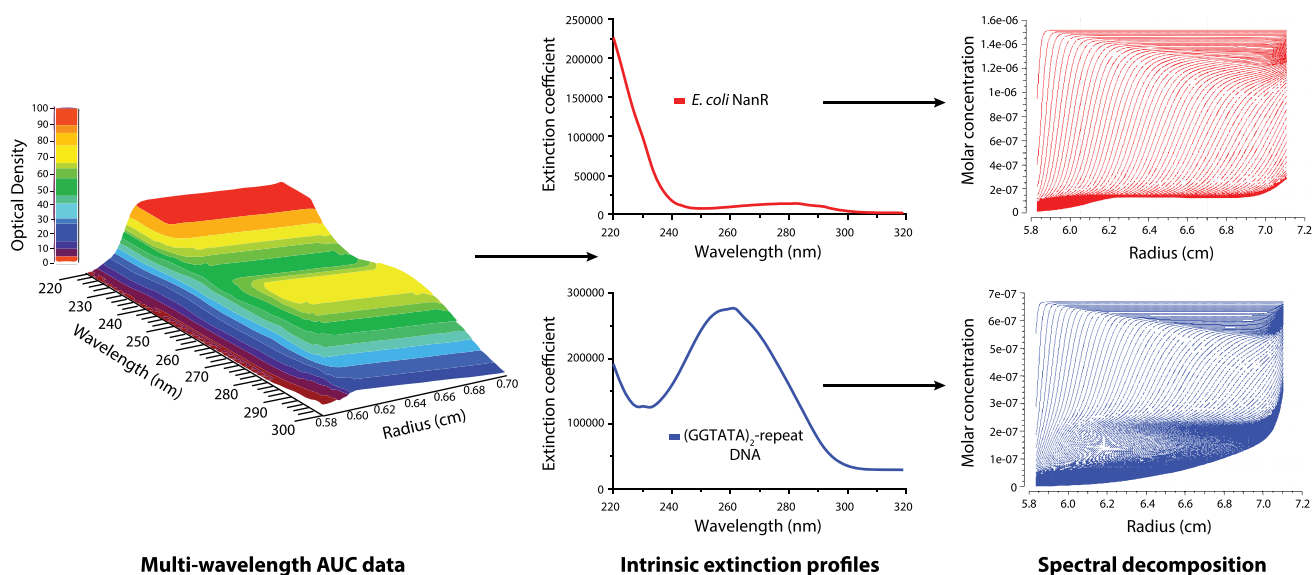


Fig. 1 Multi-wavelength analytical ultracentrifugation analysis workflow. The four-dimensional multi-wavelength AUC data (left panel, only one time point is shown) is spectrally deconvoluted with the

intrinsic extinction profile of each interaction partner (center panel) to generate datasets for the NanR and DNA components (right panel) using the non-negatively constrained least squares algorithm

directly provide the molar stoichiometry of the NanR–DNA hetero-complexes. A summary of these integration results is shown in Table 1. All figures were prepared using UltraScan and Prism 8 (GraphPad Software Inc.).

Determination of weight-averaged partial specific volume

To determine the molar mass of each species in solution, a weight-averaged partial specific volume was estimated for each complex using the following equation:

$$\bar{v} = \frac{M_1 \bar{v}_1 + M_2 \bar{v}_2}{M_1 + M_2}$$

Here, the molar mass, measured in Daltons, is required for the NanR (M_1) and DNA (M_2) components, along with the partial specific volume of NanR (\bar{v}_1) and DNA (\bar{v}_2). Molar masses of 59 kDa, 118 kDa and 177 kDa were used for the NanR-dimer₁, NanR-dimer₂ and NanR-dimer₃ protein components, respectively. A molar mass of 11.5 kDa was used for the (GGTATA)₂-repeat oligonucleotide. The partial specific volume used for NanR (\bar{v}_1) was 0.7295 mL g⁻¹, while the partial specific volume used for DNA (\bar{v}_2) was 0.55 mL g⁻¹.

Results

We first conducted control experiments by measuring purified NanR and DNA separately using sedimentation velocity (Fig. 2a, which demonstrates that NanR is dimeric (blue

trace, peak at 3.7 S; see also Table 1, below) with no evidence of self-association, an assertion further supported by the single monodisperse peak evident during size-exclusion chromatography (Supplementary Figure S1). The double-stranded DNA was largely monodisperse (orange trace, peak at 2.2 S), although a minor component at 1.9 S was observed, which is likely a small amount of single-stranded DNA that we often observe and results from incomplete annealing.

When NanR was titrated (1.2–12 μM) against the (GGTATA)₂-repeat DNA (1.2 μM), the deconvoluted sedimentation profiles for the titration series demonstrated that the NanR and DNA signals co-migrated (Fig. 2b–f), consistent with the formation of hetero-complexes. Integrating the co-migrating peaks between 4 and 5 S from the 1.2, 2.4 and 4.8 μM titration data (Fig. 2b–d) gave molar ratios of 2.1:1, 2.84:1 and 2.58:1, respectively. These molar ratios provide direct access to the stoichiometry and suggested that a single dimer of NanR was bound to DNA, consistent with the formation of a NanR-dimer₁/DNA hetero-complex. At a NanR concentration of 4.8 μM (Fig. 2d), we also observed the formation of a broad reaction boundary and two new peaks centred at 6.51 S and 8.25 S. This feature indicates sub-saturation of the hetero-complex, representing multiple and dynamic intermediate species that are mediated by mass action effects, much like the observations shown by us (Horne et al. 2020; Zhang et al. 2017). Consequently, peak integration at these regions serves as an average of the species present and, therefore, gives rise to non-integral molar ratios. Integration of the first co-migrating peak resulted in a molar ratio of 4.02:1, while integration across the second

Table 1 Integration results from the multi-wavelength AUC analysis of separated NanR and (GGTATA)₂-repeat DNA signals

	NanR		(GGTATA) ₂ -repeat DNA		NanR:(GGTATA) ₂ -repeat DNA					
	1:1	2:1	4:1 (species 1)	4:1 (species 2)	4:1 (species 3)	6:1 (species 1)	6:1 (species 2)	10:1		
Sed. coefficient (× 10 ⁻¹³ S) ^a	3.76 (3.51, 4.01)	4.39 (4.13, 4.57)	4.41 (3.91, 4.91)	4.40 (4.26, 4.55)	8.25 (7.07, 10.70)	6.26 (5.99, 6.54)	8.61 (8.34, 8.87)	8.78 (8.00, 9.56)		
Dif. coefficient (× 10 ⁻⁰⁷ D) ^a	6.3 (3.84, 8.76)	4.13 (3.67, 4.59)	5.1 (4.30, 5.89)	4.49 (3.51, 5.47)	N/D ^b	N/D ^b	3.74 (2.19, 5.3)	4.24 (4.16, 4.32)		
Measured molar ratio ^c	n/a	2.10	2.84	2.58	6.85	4.23	6.33	6.48		
Weight-averaged \bar{v} (mL g ⁻¹) ^d	0.730	0.700	0.700	0.700	0.719	0.714	0.719	0.719		
Measured molar mass (kDa) ^e	54.0 (30.0, 77.9)	86	73.1	79.4	N/D ^b	N/D ^b	148.6	178.6		
Theoretical molar mass (kDa) ^f	59	70.5	70.5	70.5	129.5	129.5	129.5	188.5	188.5	188.6
Oligomeric state of hetero-complex	n/a	n/a	Dimeric	Dimeric	Dimeric	Tetrameric	Hexameric	Tetrameric	Hexameric	Hexameric

^aThese are the sedimentation and diffusion coefficients observed following 2DSA-Monte Carlo analysis. Parameters are obtained from integration of pseudo-3D plots within the UltraScan software. All measured values represent the mean from the Monte Carlo analysis. The values in parentheses are the 95% confidence intervals from the Monte Carlo analysis

^bN/D = not determined as species were present within a reaction boundary

^cPartial concentration is determined from peak integration of the co-migrating species in both the NanR and DNA datasets. As the data is scaled to molar concentration these concentrations can be used directly to infer the molar ratio and thus stoichiometry of the complex

^dPartial specific volume (\bar{v}) of the complex, estimated from the weight-average of the protein and DNA components. A \bar{v} of 0.7295 mL g⁻¹ was used for NanR, while a \bar{v} of 0.55 mL g⁻¹ was used for DNA. The equation used to calculate the weight-averaged \bar{v} is presented in the “Materials and methods”

^eThe measured molar mass is estimated based on the hydrodynamic parameters (sedimentation and diffusion coefficient) and the weighted-averaged \bar{v} , calculated using the measured molar ratio. The values in parentheses are the 95% confidence intervals from the Monte Carlo analysis for the pure components

^fThe theoretical mass is predicted based upon the amino acid or nucleic acid sequence within UltraScan. The mass of each hetero-complex is predicted based on the observed molar ratio

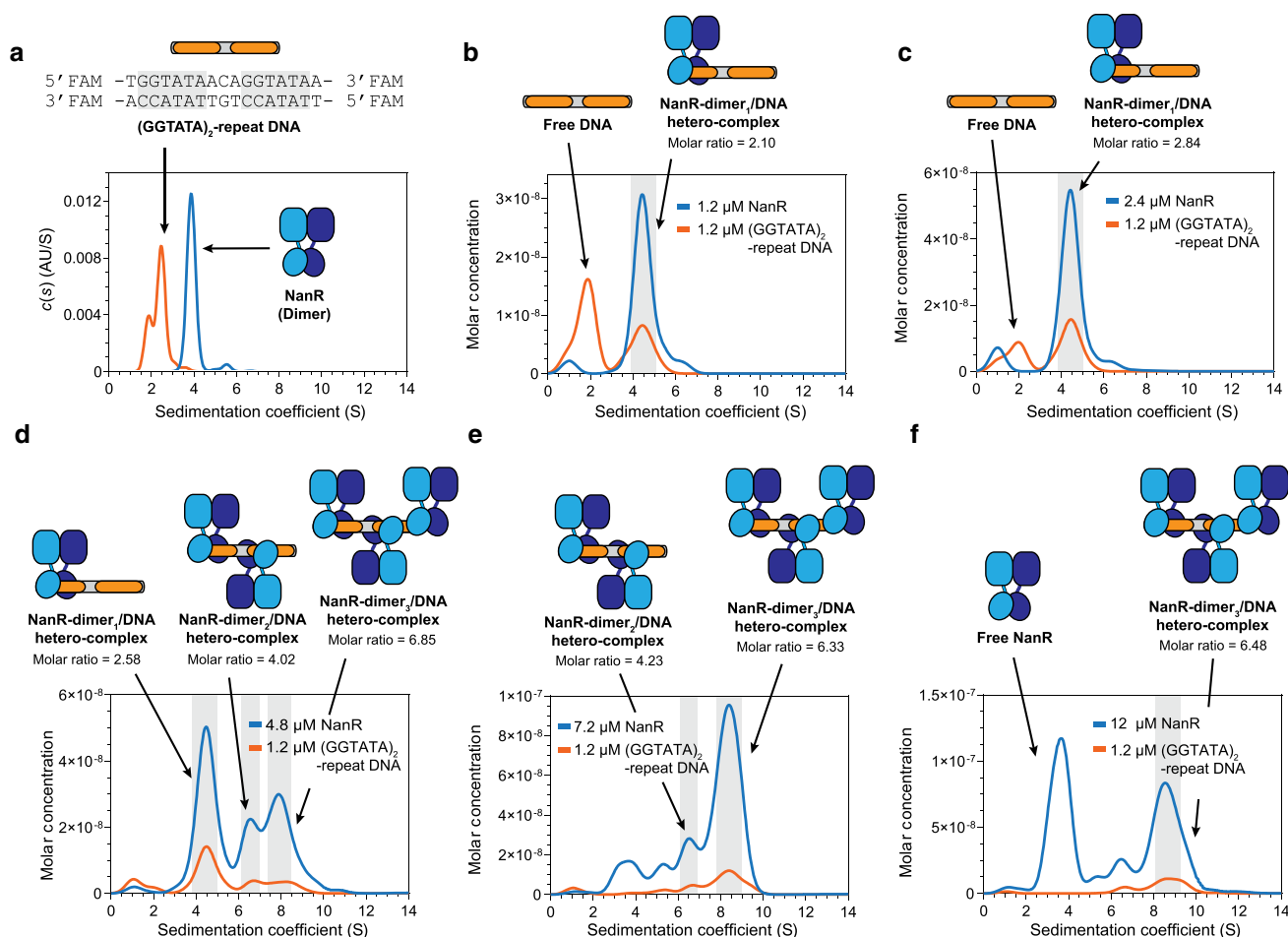


Fig. 2 The stoichiometry of the NanR–DNA hetero-complex. The deconvoluted sedimentation coefficient distributions for the NanR titration series are presented with (GGTATA)₂-repeat DNA concentration held at 1.2 μM. **a** Separate controls of NanR (12 μM, blue) and (GGTATA)₂-repeat DNA (1.2 μM, orange). **b** 1.2 μM NanR. **c** 2.4 μM NanR. **d** 4.8 μM NanR. **e** 7.2 μM NanR. **f** 12 μM NanR. Upon increasing protein concentration, a clear shift in the sedimentation coefficient is observed, consistent with the formation of higher-order hetero-complexes. The molar ratio of the integrated peaks (shaded in grey) is shown, while the oligomeric state of each hetero-complex is

depicted by schematic. The presence of excess protein, free of any co-migrating DNA in **f** indicates that hetero-complex formation has reached saturation. The broad reaction boundary is indicative of tight binding and represents multiple, dynamic intermediate species that are mediated by mass action. The presence of excess protein, free of any co-migrating DNA indicates that hetero-complex formation has reached saturation. All plots are presented as $g(s)$ distributions with the molar concentration for each interacting partner (protein and DNA) plotted on the y-axis. Spectral information and hydrodynamic parameters are detailed in Table 1

peak resulted in a molar ratio of 6.33:1, consistent with a NanR-dimer₂/DNA and NanR-dimer₃/DNA hetero-complex, respectively. As the concentration of NanR was increased to 7.2 μM (Fig. 2e), the molar ratio of both NanR-dimer₂/DNA and NanR-dimer₃/DNA hetero-complex did not change, however, the sedimentation distribution of the reaction boundary considerably narrowed towards the peak centred at 8.61 S. Upon increasing the concentration of NanR further to 12 μM (Fig. 2f), this trend for increasing NanR-dimer₃/DNA hetero-complex remained, and the appearance of a peak corresponding to free protein at ~3.9 S was observed, indicating that the system had reached saturation.

Through transformation of the hydrodynamic data and an associated weight-averaged partial specific volume, we

also measured molar mass values for the NanR-dimer₁/DNA and NanR-dimer₃/DNA hetero-complex that were in excellent agreement with their theoretical molar mass (Table 1), which therefore corroborate the molar stoichiometry above. As the peak centred at ~6.4 S lies within the reaction boundary, an accurate molecular weight for the NanR-dimer₂/DNA hetero-complex could not be determined. Detailed results of the stoichiometry and hydrodynamic properties are listed in Table 1.

To corroborate the multi-wavelength AUC experiments, we performed an electrophoretic mobility shift assay (EMSA) using fluorescently labelled (GGTATA)₂-repeat DNA. Titrating NanR against this FAM-5'-labelled oligonucleotide resulted in the formation of two

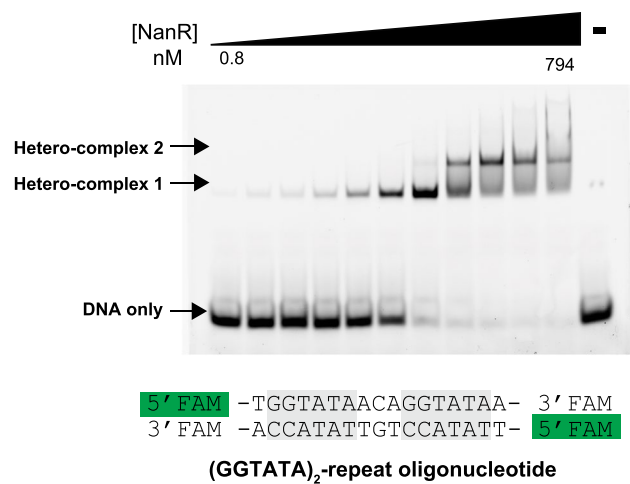


Fig. 3 EMSA of NanR titrated against fluorescently labelled (GGTATA)₂-repeat DNA. Two concentration-dependent hetero-complexes are observed when two GGTATA repeats are present

concentration-dependent hetero-complexes (Fig. 3). This is largely consistent with the multi-wavelength AUC experiment; however, we do not specifically observe the formation of the highest-order hetero-complex (NanR-dimer₃/DNA hetero-complex). Instead, at the highest concentration of NanR (794 nM), we see an extended smear on the gel. This absence in the EMSA suggests that the label-free oligonucleotide used in the AUC experiment may be sterically unhindered and hence NanR could form protein-mediated bridges between oligonucleotides via each NanR monomer. Alternatively, it may reflect altered binding conditions of the AUC experiment *vs.* the EMSA, in which there is a significantly decreased salt concentration.

Discussion

We investigated the nature of the NanR–DNA interaction, label-free and in solution by multi-wavelength sedimentation velocity experiments. Through spectral decomposition of the NanR and DNA signals, we determined that dimers of NanR sequentially bind each GGTATA repeat and found that hetero-complex formation is concentration-dependent. This analysis was complemented by traditional hydrodynamic information. Furthermore, the observation of a multimeric assembly process suggests that the NanR-dimer₁/DNA hetero-complex plays an integral role in the formation of the higher-order hetero-complexes, which proceeds through a broad reaction boundary before reaching saturation.

The presence of multiple species at low protein concentration indicates sub-saturation of the hetero-complex, representing multiple and dynamic intermediate species that are mediated by mass action effects, much like the observations

shown by us (Horne et al. 2020; Zhang et al. 2017); . We note that DNA was always present in sub-stoichiometric amounts, and therefore was always consumed by NanR binding as dimers to the DNA; hence, free DNA was never observed within this reaction boundary. The absence of free DNA suggests that the K_D for this assembly process is very low, which is consistent with the nanomolar affinity defined in our previous study for the (GGTATA)₃-repeat operator sequence (Horne et al. 2020). Consequently, the dissociation constant for this system is well below the detection capacity of the Optima AUC.

Lastly, this work provides a good example of the utility of multi-wavelength AUC and we are very happy to make this data available to the community as an example dataset for training others in this new technique.

Conclusion

In addition to protein–DNA interactions, multi-wavelength AUC can be used to characterize any interacting system within a complex mixture, providing the interaction partners can be spectrally decomposed based on their unique optical properties. This provides both hydrodynamic and spectral characterization of an interacting system to define the stoichiometry of association. The additional spectral dimension featured in these experiments opens the door for many new applications where interactions between dissimilar molecules can be measured with high resolution—such as peptides, nanoparticles, antibody–drug conjugates, heme groups, or fluorescently-tagged molecules [for representative studies, we refer the reader to Johnson et al. (2018), Mitra and Demeler (2020), Schneidewind et al. (2019) and Wawra et al. (2018)]. To that end, this next-generation approach promises to be the method of choice for analysing complex interactions that comprise different types of biomolecules to unlock a wealth of new research that previously was inaccessible.

Acknowledgements We are grateful to the New Zealand Royal Society Marsden Fund (RCJD, UOC1506); Ministry of Business, Innovation and Employment Smart Ideas Grant (RCJD, UOCX1706); and the National Institutes of Health Grants (BD, GM120600 and NSF-ACI-1339649). We acknowledge grant support for CRH (Maurice Wilkins Centre). MWL-AUC experiments were performed at the Canadian Center for Hydrodynamics, University of Lethbridge with support from the Canada Foundation for Innovation Grant CFI-37589. UltraScan multi-wavelength development is supported by NIH Grant GM120600 (BD), UltraScan supercomputer calculations were supported through NSF/XSEDE Grant TG-MCB070039N (BD), and University of Texas Grant TG457201 (BD).

Author contributions CRH designed and performed experiments, and analysed data with support in data interpretation from AH and BD. RCJD supervised the project and co-wrote the paper with CRH. All authors commented on the manuscript.

Compliance with ethical standards

Conflict of interest The authors declare no conflicts of interest.

References

- Almagro-Moreno S, Boyd EF (2009) Insights into the evolution of sialic acid catabolism among bacteria. *BMC Evol Biol* 9:118
- Baos SC, Phillips DB, Wildling L, McMaster TJ, Berry M (2012) Distribution of sialic acids on mucins and gels: a defense mechanism. *Biophys J* 102:176–184
- Berke IC, Modis Y (2012) MDA5 cooperatively forms dimers and ATP-sensitive filaments upon binding double-stranded RNA. *EMBO J* 31:1714–1726
- Bervoets I, Charlier D (2019) Diversity, versatility and complexity of bacterial gene regulation mechanisms: opportunities and drawbacks for applications in synthetic biology. *FEMS Microbiol Rev* 43:304–339
- Brookes E, Cao WM, Demeler B (2010) A two-dimensional spectrum analysis for sedimentation velocity experiments of mixtures with heterogeneity in molecular weight and shape. *Eur Biophys J Biophys* 39:405–414
- Cole JL, Lary JW, T PM, Laue TM, (2008) Analytical ultracentrifugation: sedimentation velocity and sedimentation equilibrium. *Methods Cell Biol* 84:143–179
- Coombes D, Davies JS, Newton-Vesty MC, Horne CR, Setty TG, Subramanian R, Moir JWB, Friemann R, Panjikar S, Griffin MDW, North RA, Dobson RCJ (2020) The basis for non-canonical ROK family function in the *N*-acetylmannosamine kinase from the pathogen *Staphylococcus aureus*. *J Biol Chem* 295:3301–3315
- Davies JS, Coombes D, Horne CR, Pearce FG, Friemann R, North RA, Dobson RCJ (2019) Functional and solution structure studies of amino sugar deacetylase and deaminase enzymes from *Staphylococcus aureus*. *FEBS Lett* 593:52–66
- de Lorenzo V, Cases I (2005) Promoters in the environment: transcriptional regulation in its natural context. *Nat Rev Microbiol* 3:105–118
- Demeler B (2010) Methods for the design and analysis of sedimentation velocity and sedimentation equilibrium experiments with proteins. *CurrProtoc Protein Sci Chapter 7:Unit 7.13*
- Demeler B, Gorbet G (2016) Analytical ultracentrifugation data analysis with ultrascan-iii, Ch 8. In: Uchiyama S, Stafford WF, Laue T (eds) *Analytical ultracentrifugation: instrumentation, software, and applications*. Springer, 119–143 (2016)
- Demeler B, Brookes E, Nagel-Steger L (2009) Analysis of heterogeneity in molecular weight and shape by analytical ultracentrifugation using parallel distributed computing. *Methods Enzymol* 454:87–113
- Deutscher J (2008) The mechanisms of carbon catabolite repression in bacteria. *Curr Opin Microbiol* 11:87–93
- Fasman G (1975) In handbook of biochemistry and molecular biology, nucleic acids, vol I. Chem. Rubber Co, Cleveland, pp 76–206
- Gerosa L, Kochanowski K, Heinemann M, Sauer U (2013) Dissecting specific and global transcriptional regulation of bacterial gene expression. *Mol Syst Biol* 9:658
- Gorbet GE, Pearson JZ, Demeler AK, Cölfen H, Demeler B (2015) Next-generation AUC: analysis of multiwavelength analytical ultracentrifugation data. *Methods Enzymol* 562:27–47
- Gorke B, Stulke J (2008) Carbon catabolite repression in bacteria: many ways to make the most out of nutrients. *Nat Rev Microbiol* 6:613–624
- Horne CR, Kind L, Davies JS, Dobson RCJ (2020) On the structure and function of *Escherichia coli* YjhC: An oxidoreductase involved in bacterial sialic acid metabolism. *Proteins* 88:654–668
- Horne CR, Venugopal H, Panjikar S, Henrickson A, Brookes E, North RA, Murphy JM, Friemann R, Griffin MDW, Ramm G, Demeler B, Dobson RCJ (2020) Mechanism of NanR gene repression and allosteric induction of bacterial sialic acid metabolism. *bioRxiv:2020.2004.2022.056440*
- Johnson CN, Gorbet GE, Ramsower H, Urquidi J, Brancalione L, Demeler B (2018) Multi-wavelength analytical ultracentrifugation of human serum albumin complexed with porphyrin. *Eur Biophys J* 47:789–797
- Kalivoda KA, Steenbergen SM, Vimr ER, Plumbridge J (2003) Regulation of sialic acid catabolism by the DNA binding protein NanR in *Escherichia coli*. *J Bacteriol* 185:4806–4815
- Kroe RR, Laue TM (2009) NUTS and BOLTS: applications of fluorescence-detected sedimentation. *Anal Biochem* 390:1–13
- Laue TM, Sear DF, Eaton S, Ross JB (1993) 5-hydroxytryptophan as a new intrinsic probe for investigating protein–DNA interactions by analytical ultracentrifugation. Study of the effect of DNA on self-assembly of the bacteriophage lambda cI repressor. *Biochemistry* 32:2469–2472
- Lawson CL, Hanson RJ (1974) Solving least squares problems. Prentice-Hall Inc, Englewood Cliffs
- Lee SP, Fuior E, Lewis MS, Han MK (2001) Analytical ultracentrifugation studies of translin: analysis of protein–DNA interactions using a single-stranded fluorogenic oligonucleotide. *Biochemistry* 40:14081–14088
- MacGregor IK, Anderson AL, Laue TM (2004) Fluorescence detection for the XLI analytical ultracentrifuge. *Biophys Chem* 108:165–185
- Mitra S, Demeler B (2020) Probing RNA–protein interactions and RNA compaction by sedimentation velocity analytical ultracentrifugation. *Methods Mol Biol (Clifton, NJ)* 2113:281–317
- North RA, Watson AJ, Pearce FG, Muscroft-Taylor AC, Friemann R, Fairbanks AJ, Dobson RC (2016) Structure and inhibition of *N*-acetylneuraminidase from methicillin-resistant *Staphylococcus aureus*. *FEBS Lett* 590:4414–4428
- North RA, Horne CR, Davies JS, Remus DM, Muscroft-Taylor AC, Goyal P, Wahlgren WY, Ramaswamy S, Friemann R, Dobson RCJ (2018) “Just a spoonful of sugar...”: import of sialic acid across bacterial cell membranes. *Biophys Rev* 10:219–227
- North RA, Wahlgren WY, Remus DM, Scalise M, Kessans SA, Dunevall E, Claesson E, Soares da Costa TP, Perugini MA, Ramaswamy S, Allison JR, Indiveri C, Friemann R, Dobson RCJ (2018) The sodium sialic acid symporter from *Staphylococcus aureus* has altered substrate specificity. *Front Chem* 6:233
- Pearson JZ, Krause F, Haffke D, Demeler B, Schilling K, Colfen H (2015) Next-generation AUC adds a spectral dimension: development of multiwavelength detectors for the analytical ultracentrifuge. *Methods Enzymol* 562:1–26
- Schneidewind J, Krause F, Bocola M, Stadler AM, Davari MD, Schwaneberg U, Jaeger KE, Krauss U (2019) Consensus model of a cyanobacterial light-dependent protochlorophyllide oxidoreductase in its pigment-free apo-form and photoactive ternary complex. *Commun Biol* 2:351
- Vimr ER (2013) Unified theory of bacterial sialometabolism: how and why bacteria metabolise host sialic acids. *IntSch Res Not Micro* 2013:816713
- Vimr ER, Kalivoda KA, Deszo EL, Steenbergen SM (2004) Diversity of microbial sialic acid metabolism. *Microbiol Mol Biol Rev* 68:132–153
- Wahlgren WY, Dunevall E, North RA, Paz A, Scalise M, Bisignano P, Bengtsson-Palme J, Goyal P, Claesson E, Caing-Carlsson R, Andersson R, Beis K, Nilsson UJ, Farewell A, Pochini L, Indiveri C, Grabe M, Dobson RCJ, Abramson J, Ramaswamy S, Friemann

- R (2018) Substrate-bound outward-open structure of a Na(+)-coupled sialic acid symporter reveals a new Na(+) site. *Nat Commun* 9:1753
- Wawra SE, Pflug L, Thajudeen T, Kryschi C, Stingl M, Peukert W (2018) Determination of the two-dimensional distributions of gold nanorods by multiwavelength analytical ultracentrifugation. *Nat Commun* 9:4898
- Witte G, Urbanke C, Curth U (2005) Single-stranded DNA-binding protein of *Deinococcus radiodurans*: a biophysical characterization. *Nucleic Acids Res* 33:1662–1670
- Yang TC, Catalano CE, Maluf NK (2015) Analytical ultracentrifugation as a tool to study nonspecific protein–DNA Interactions. *Methods Enzymol* 562:305–330
- Zhang J, Pearson JZ, Gorbet GE, Colfen H, Germann MW, Brinton MA, Demeler B (2017) Spectral and hydrodynamic analysis of west nile virus RNA–Protein interactions by multiwavelength sedimentation velocity in the analytical ultracentrifuge. *Anal Chem* 89:862–870
- Zhao H, Mayer ML, Schuck P (2014) Analysis of protein interactions with picomolar binding affinity by fluorescence-detected sedimentation velocity. *Anal Chem* 86:3181–3187

Publisher's Note Springer Nature remains neutral with regard to jurisdictional claims in published maps and institutional affiliations.